LAWRENCE
LIVERMORE
NATIONAL
LABORATORY

LLNL-JRNL-633354

Regulation of Electrochemically Generated Ferrous Ions from an Iron Cathode for Pd-Catalytic Transformation of MTBE in Groundwater

P. Liao, S. Yuan, M. Chen, M. Tong, W. Xie, P. Zhang

April 5, 2013

Environmental Science & Technology

Disclaimer

Regulation of Electrochemically Generated Ferrous Ions from an Iron Cathode for Pd-Catalytic Transformation of MTBE in Groundwater

Peng Liao[†], *Songhu Yuan*[*,†], *Mingjie Chen*[‡], *Man Tong*[†], *Wenjing Xie*[†], *Peng Zhang*[†]

[†]State Key Lab of Biogeology and Environmental Geology, China University of Geosciences, 388 Lumo Road, Wuhan 430074, P. R. China

[‡]Atmospheric, Earth and Energy Division, Lawrence Livermore National Laboratory, P.O. Box 808, L-184, Livermore, CA 94550, United States

*E-mail: yuansonghu622@hotmail.com; Phone: +86-27-67848629;

Fax: +86-27-67848629.

RECEIVED DATE (to be automatically inserted after your manuscript is accepted if required according to the journal that you are submitting your paper to)

ABSTRACT An effective approach is developed to regulate the generation of Fe^{2+} from an iron cathode in a three-electrode system. The Fe^{2+} is then used for the Pd-catalytic transformation of methyl *tert*-butyl ether (MTBE) in simulated groundwater. Under conditions of pH 3, a total current of 50 mA, and 1 g/L Pd/Al_2O_3, 20 mg/L MTBE was completely transformed within 60 min in an undivided electrolytic cell using the iron cathode, with 14 mg/L of accumulated Fe^{2+}. Fe^{2+} accumulation follows pseudo-first-order kinetics and the rate is regulated by electric current and groundwater pH, giving the relation of $k = 5.3 \times 10^4 \bullet 10^{-2pH} - 7.25 \bullet I^2 - 8.8 \times 10^{11} \bullet 10^{2pH-28}$, where k is the rate constant of Fe^{2+} accumulation (min^{-1}) and I is the current (mA). In a modified three-electrode column using iron as the first cathode, the localized acidic and oxidizing conditions developed automatically in the iron cathode zone by partitioning the current between the two cathodes, leading to controllable generation of Fe^{2+} for MTBE transformation. The stable transformation of MTBE in a long-term study suggests that this method is a sustainable approach to supplying Fe^{2+} for Pd-catalytic transformation of organic contaminants in groundwater.

INTRODUCTION

Methyl *tert*-butyl ether (MTBE) has been manufactured almost exclusively for use as a fuel additive since the 1970s.[1–3] MTBE has been found in various environments, particularly in groundwater, because of its high solubility under ambient conditions (48 g/L).[1] MTBE was reclassified by the USEPA as "carcinogenic in humans by all

routes of exposure" based on findings that indicated side effects of headaches, vomiting, diarrhea, fever, cough, muscle aches, and skin and eye irritation.[1,4] Current processes that have been proposed for remediation of MTBE in groundwater include phase transfer,[5] in situ chemical oxidation (ISCO),[6] advanced oxidation technologies (AOTs),[7–9] and biodegradation.[2,10,11] Electrochemical processes have attracted increasing interest in groundwater remediation as it is simple and versatile.[12–15] Recently, a hybrid electrolysis and Pd-catalytic oxidation process, in which H_2O_2 was produced from the combination of electro-generated H_2 and O_2 on a Pd catalyst under acidic conditions (eq. 1–3), has been shown to be highly effective in treating a wide range of recalcitrant contaminants in wastewaters and groundwater (eqs. 4 and 5).[12,13,16] The concentration of Fe(II) significantly affects the efficiency of the contaminant transformation,[12,13,16] and a certain amount of Fe(II) (13.7 mg/L) shifts trichloroethylene (TCE) transformation from hydrodechlorination to hydroxyl oxidation.[12] However, in situ application of this process is limited because of a lack of Fe(II) (ca. 10 mg/L), especially in iron-defective aquifers.

$$2H_2O \longrightarrow O_2 + 4H^+ + 4e^- \quad (1)$$

$$2H_2O + 2e^- \longrightarrow H_2 + 2OH^- \quad (2)$$

$$H_2 + O_2 \xrightarrow{Pd} H_2O_2 \quad (3)$$

$$H_2O_2 + Fe^{2+} + H^+ \longrightarrow Fe^{3+} + \bullet OH + H_2O \quad (4)$$

$$Orgs + \bullet OH \longrightarrow \text{Oxidation products} \quad (5)$$

Fe(II) is normally supplied by the addition of ferrous salts,[17,18] sacrificed iron anode,[19,20] and iron-containing minerals in Fenton-based processes.[21,22] The addition

of ferrous salts complicates the implementation process. Sacrificial iron anodes can be effective (eq. 6) but produce a lot of iron sludge.[23] When iron is used as the anode, it corrodes and no O_2 is produced. Therefore, there will be a lack of O_2 for H_2O_2 production as O_2 is a necessary reactant. Although iron-containing materials, such as Fe_3O_4 and zero-valency iron (ZVI), can be mixed with Pd to supply Fe(II), the reaction will deplete the materials,[24,25] and precipitates on the Pd surface will decrease the catalytic activity and clog the aquifer.[26–28] Therefore, it is crucial to seek a new cost-effective strategy to supply Fe(II) for the hybrid electrolysis and Pd-catalytic oxidation process.

$$Fe - 2e^- \longrightarrow Fe^{2+} \quad (6)$$

$$Fe + 2H^+ \longrightarrow Fe^{2+} + H_2 \quad (7)$$

During the process, localized acidic conditions in the vicinity of Pd automatically develops in a modified three-electrode system as there are more H^+ ions produced at the anode than OH^- ions produced at the adjacent cathode.[13,16] One anode and two cathodes aim to sustain water electrolysis, thus supplying H_2, O_2, H^+ and OH^- for H_2O_2 production on the Pd surface (eqs. 1–3).[13,16] Therefore, it is not feasible to change the electrochemical reactions at the three electrodes. However, the chemical reactions at the electrodes will still occur regardless of whether or not electricity is applied. For example, chemical corrosion of iron occurs naturally, though it is particularly intensive under acidic conditions (eq. 7).[29] When the iron is used as the first cathode in the three-electrode system,[13] the chemical corrosion is enhanced under the automatically developed acidic conditions. However, the corrosion is inhibited by

a negative applied current that protects the cathode.[30–32] Consequently, using iron as the first cathode does not change the electrochemical reactions (eqs. 1–3), but supplies Fe(II) due to chemical corrosion under acidic conditions (eq. 7). The production of Fe(II) from the iron cathode can be theoretically regulated by conditioning the cathodic current.

In this study, an undivided electrolytic cell with an iron cathode is used to regulate the generation of Fe^{2+} at different values of pH and current for Pd-catalytic transformation of MTBE in simulated groundwater. The kinetics and mechanism of Fe^{2+} accumulation are also explored. The relation of Fe^{2+} accumulation with pH and cathodic current is modeled. A modified three-electrode column using an iron cathode is then configured to regulate Fe^{2+} accumulation by varying the cathodic current applied on the iron cathode for transformation of MTBE. The long-term performance of this column is ultimately evaluated.

EXPERIMENTAL

Chemicals. MTBE (99.8%) and *tert*-butyl alcohol (TBA, 99.5%) were purchased from Sigma-Aldrich. *Tert*-butyl formate (TBF, 99.5%), acetone (AC, 99.5%), formaldehyde (FA, 37%), and formic acid (99.5%) were supplied by Aladdin Chemistry Co. Ltd. Palladium on alumina powder (5% wt. Pd, Shanxi Kaida Chemical Ltd, China), with an average particle size of 6 μm, was used as the catalyst in the batch experiments. Palladium on alumina pellets (0.5% wt. Pd, Shanxi Kaida Chemical Ltd) 4 mm in size was used in the column experiments. Iron plate (S45C

type, Wuhan Steel Processing Co., Ltd, China) and mixed metal oxides (MMO, IrO_2 and Ta_2O_5 coating on titanium diamond mesh, Shanxi Kaida Chemical Ltd) with dimensions of 5.0 cm diameter and 1.7 mm thickness were used as the electrodes. Seventeen holes (4.1 mm in diameter) were evenly distributed through the iron plate electrodes. Prior to the experiments, the iron electrode was polished with coarse emery cloth, etched by diluted HCl solution (5 wt %), and washed with deionized water. Deionized water (18.2 mΩ·cm) obtained from a Millipore Milli-Q system was used in all the experiments. All the chemicals used in this study were above analytical grade.

Batch Experiments. An undivided acrylic electrolytic cell was used to evaluate Fe^{2+} generation for MTBE transformation at ambient temperatures (25 ± 1 °C) (Figure S1 in the Supporting Information). An MMO mesh and an iron plate were respectively used as the anode and cathode, with 40 mm spacing in parallel positions. For each test, 400 mL of 20 mg/L MTBE solution was transferred into the cell, and 10 mM Na_2SO_4 and 1 g/L Pd/Al_2O_3 (5% wt. Pd) were attained by the addition of specific masses of Na_2SO_4 and Pd/Al_2O_3 powder. Aqueous pH was adjusted to 3.0 by 1 M H_2SO_4. For comparison, an MMO mesh was used as the cathode in the presence of 10 mg/L Fe^{2+}. The reactor was immediately sealed and stirred at 600 rpm using a Teflon-coated magnetic stirring bar. A constant electric current of 50 mA (2 mA/cm^2) was applied with a cell potential of about 4 V. The aqueous solution was sampled at pre-determined time intervals for analysis of MTBE and its transformation products, iron species, pH, H_2O_2, and •OH concentration. All experiments were carried out in

duplicate.

Column Experiments. A vertical acrylic tube column (5.0 cm inner diameter × 30 cm length) was used to simulate one-dimensional flow conditions (Figure 1). Three electrodes were mounted in the upward sequence of anode (MMO), cathode 1 (iron plate) and cathode 2 (MMO). 4.5 g of Pd/Al_2O_3 pellets were supported by cathode 1 to produce a pellet bed monolayer. The remaining space in the column was packed with 4 mm glass beads with a porosity of 0.46. The total and pore volume (PV) were 588 and 268 mL, respectively. Solution was pumped through the bottom of the columns at a rate of 2.5 mL/min using a peristaltic pump (Luxi, model HL-2, China). The flow rate was maintained at 2.5 mL/min, resulting in Darcy's velocity of 1.83 m/day. The total current was kept at 80 mA by a DC power supply (GPC-3060D, Taiwan Goodwill Instrument). By adjusting the rheostat, different currents were partitioned between cathodes 1 and 2 so that the localized pH in the Pd vicinity could be regulated. Simulated MTBE-contaminated groundwater (10 mg/L) with 5 mM Na_2SO_4 and 0.5 mM $CaSO_4$ deoxygenated solution (~ 840 μS/cm) was stored in a 5 L gas-tight collapsible bag. The column was flushed by 2 PVs of contaminated groundwater before switching on the power supply. Control experiments show that the adsorption of MTBE on Pd/Al_2O_3 pellets and glass beads were negligible during operation. At regular time intervals, 1 mL of groundwater was sampled from six ports (see Figure 1 for locations) and measured for MTBE, pH, and iron species concentration.

Chemical Analysis. MTBE, TBF, TBA, and AC concentrations were analyzed

using a gas chromatograph (GC, Shimadzu 2014C, Japan) equipped with a flame ionization detector (FID), a capillary column (30 m × 0.32 mm × 0.5 μm) and a headspace concentrator (DK-3001A, Beijing Zhongxing Huili Technology Development Co., Ltd.). The column temperature was held at 35 °C for 2 min, heated from 35 to 60 °C at a rate of 5 °C/min, and then cooled to 35 °C at a rate of 10 °C/min. The injector and detector temperatures were set at 220 and 250 °C, respectively. 2 mL of the aqueous sample was collected and injected into a 20-mL headspace vial sealed with septa. The equilibrium temperature in the vial was set to 105 °C. The detection limits for all compounds were 0.1 mg/L. Gas concentrations were calculated by Henry's law. FA was analyzed by an LC-15C HPLC (Shimadzu) equipped with a UV detector and an XDB-C18 column (4.6 × 50 mm) after derivatization with 2,4-dinitrophenylhydrazine.[33] The mobile phase used a mixture of acetonitrile and water (60:40, v/v) at 1 mL/min, with the detection wavelength at 355 nm. Carboxylic acids were also measured by HPLC. The mobile phase used a mixture of phosphoric buffer (pH 2.7) and methanol at 99:1 (v:v) at 0.8 mL/min, and a detection wavelength of 210 nm. The detection limits for FA and carboxylic acids were 1 μM.

H_2O_2 concentration was determined at 405 nm by a spectrometer (UV-1800 PC, Shanghai Mapada Spectrum Instrument Co., Ltd) after coloration with $TiSO_4$.[34] The •OH levels were determined using dimethyl sulfoxide (DMSO) trapping and HPLC methods described in previous literature.[35] Iron species were measured at 510 nm using the 1,10-o-phenanthroline analytical method.[36] The corrosion potentials of the iron electrode at various pH and at 50 mA were measured on a CS150 electrochemical

175 workstation (Wuhan CorrTest Instrument, China) using a Pt electrode as the counter
176 electrode and a saturated calomel electrode (SCE) as the reference electrode. The
177 electrolyte used for measurement was 10 mM $NaSO_4$.

178

179 RESULTS AND DISCUSSION

180 **Generation of Fe^{2+} from Iron Cathode for MTBE Transformation.** Figure 2a
181 shows the variation in the MTBE concentration in an undivided electrolytic cell using
182 an iron cathode under conditions of pH 3, 50 mA and 1 g/L Pd/Al_2O_3. The control
183 experiment using the iron cathode without an applied current or Pd catalyst does not
184 present any significant transformation of MTBE. In the presence of Pd/Al_2O_3, MTBE
185 (20 mg/L) was completely transformed in 60 min following pseudo-first-order
186 kinetics with a rate constant of 0.040 min^{-1}. For comparison, the experiment also used
187 an MMO cathode in the presence of 10 mg/L Fe^{2+}, which is the average concentration
188 accumulated in the cell using the iron cathode. This showed a slower MTBE
189 transformation with a pseudo-first-order rate constant of 0.036 min^{-1}. These results
190 prove that it is feasible to generate Fe^{2+} ions from an iron cathode for Pd-catalytic
191 transformation of organic contaminants in groundwater.

192 The concentration of Fe^{2+} increases to a plateau at about 14 mg/L within 60 min of
193 using the iron cathode, and decreases from the initial 10 mg/L to 8 mg/L using the
194 MMO cathode (Figure 2b). The solution pH increased from 3.0 to 3.3 using the iron
195 cathode. A parallel test using the MMO cathode had minimal variation of the pH. The
196 pH increase is attributed to the consumption of H^+ ions by chemical corrosion of the

197 iron cathode (eq. 7). The concentration of Fe^{2+} released from chemical corrosion due
198 to a rise in the pH was calculated to be 14 mg/L within 60 min, which is in good
199 agreement with the measured cumulative concentration. In addition, the corrosion
200 potential (Eh) of the iron electrode under conditions of pH 3 and 50 mA was measured
201 to be –0.440 V (Figure S2a), falling in the corrosion region (Figure S2b). As a result,
202 chemical corrosion of the iron cathode is responsible for Fe^{2+} generation under the
203 protection of cathodic current.

204 The cumulative H_2O_2 concentration reaches approximately 14 mg/L within 60 min
205 in the presence of Pd/Al_2O_3 and absence of Fe^{2+} (Figure S3). The cumulative
206 concentration of •OH radicals (oxidation potential: 2.8V/SHE) increases for both
207 systems using the iron and MMO cathodes (Figure S4). Good correlation between
208 MTBE transformation rate constants and •OH generation rate constants (Figure S5)
209 indicates that •OH was responsible for MTBE transformation ($k_{MTBE\text{-}\bullet OH}$ = 1.6 × 10^9
210 M^{-1} s^{-1} [1]).[12] The combination of H_2O_2 and Fe^{2+} produces •OH radicals for MTBE
211 oxidation (eqs. 4 and 5).[1,17,18] The ratio of H_2O_2 to Fe^{2+} is critical for the
212 transformation efficiency.[17,37] H_2O_2 and Fe^{2+} were generated gradually using the iron
213 cathode. In the cell using the MMO cathode, Fe^{2+} concentration was in excess relative
214 to the H_2O_2 concentration during the first stage, but was defective in the later stage. In
215 this regard, using an iron cathode is advantageous over the external addition of Fe(II)
216 in terms of Fe^{2+} supply.

217 During the transformation of MTBE using the iron cathode, the primary
218 transformation intermediates identified are TBF, followed by AC, TBA, FA, and

219 formic acid (Figure S6). The relatively low mass balance of carbon (65%) suggests
220 the production of CO_2.[12] Accumulation of intermediates is due to their low reaction
221 rates with •OH, which are one or two orders of magnitude lower than that of MTBE.[38]
222 It should be noted that the toxicities of the intermediates are lower than that of
223 MTBE.[39] The intermediates identified in this study are similar to those reported in
224 MTBE oxidation by anodic Fenton[40] and UV/H_2O_2.[8]

225 **Kinetic Model for Fe^{2+} Accumulation.** When electricity is applied to the iron
226 cathode, accumulation of Fe^{2+} depends on the current and solution pH. The decreasing
227 solution pH increases the rate of chemical corrosion of the iron cathode (eq. 7).[29] The
228 increasing current increases the electron density on the iron cathode, which suppresses
229 the release of electrons from the iron corrosion (reverse reaction of eq. 6).[30,42] The
230 accumulation of Fe^{2+} also decreases at high pH due to precipitation (eq. 8). If the
231 reductive regeneration of Fe^{2+} on the iron cathode is neglected, the rate of Fe^{2+}
232 accumulation using an iron cathode in the absence of Pd/Al_2O_3 can be expressed as eq.
233 9.

234 $$Fe^{2+} + 2OH^- \longrightarrow Fe(OH)_2 \qquad pK_{sp} = 16.31 \qquad (8)$$

235 $$\frac{d[Fe(II)]}{dt} = k_{H^+} \bullet [H^+]^2 \bullet [Fe] - k_{e^-} \bullet [n_{e^-}]^2 \bullet [Fe^{2+}] - k_{OH^-} \bullet [OH^-]^2 \bullet [Fe^{2+}] \qquad (9)$$

236 Where k_{H^+}, k_{e^-} and k_{OH^-} are the rate constants for Fe^{2+} generation by H^+ and $[n_{e^-}]$ is the
237 electron density concentration.

238 $$[H^+] = 10^{-pH} \qquad (10)$$

239 $$[OH^-] = 10^{pH-14} \qquad (11)$$

240 $$[n_{e^-}] = dn/dt = (L \bullet I/N_A)/V \qquad (12)$$

Where L is the quantity of electricity per unit time (6.24×10^{18}), N_A is the Avogadro constant (6.02×10^{23}), and V is the electrolyte volume (0.4 L in this study). Since the concentration of Fe (expressed by surface area) is linearly related with Fe^{2+} (Figure S7), eq. 9 can be re-written as

$$\frac{d[Fe(II)]}{dt} = (k_H^{+'} \cdot 10^{-2pH} - k_e^- \cdot k' \cdot I^2 - k_{OH}^- \cdot 10^{2pH-28}) \cdot [Fe^{2+}]$$

$$= k \cdot [Fe^{2+}] \quad (13)$$

where k ($= k_H^{+'} \cdot 10^{-2pH} - k_e^- \cdot k' \cdot I^2 - k_{OH}^- \cdot 10^{2pH-28}$) is the final accumulation rate of Fe^{2+}, and k' ($= C^2/N_A^2 \cdot V^2$) is a constant ($= 6.7 \times 10^{-10}$). The accumulation of Fe^{2+} conforms to pseudo-first-order kinetics, and the rate constant can be quantitatively regulated by electric current and solution pH.

Effects of Current and pH on Fe^{2+} Accumulation. Figure 3 displays the variation of Fe^{2+} concentration at different currents and pHs using the iron cathode. The values of $k_H^{+'}$, k_e-, and k_{OH}^- were calculated to be 5.3×10^4, 1.08×10^{10}, and 8.8×10^{11} M^{-1} s^{-1} at pH 2 without electricity application, at pH 3 and 50 mA current, and at pH 5 and 50 mA current, respectively.[43] At pH 3, the accumulation of Fe^{2+} at different currents approximately follows pseudo-first-order kinetics. A quantitative relationship between k and current was obtained as $k = 0.053 - 7.25 \cdot I^2$ when pH = 3 is set in eq. 13. It can be seen that the k value decreases quadratically with increasing the current. The rate constant of Fe^{2+} accumulation decreases from 0.052 min^{-1} without an applied current to 0.005 min^{-1} at 80 mA (inset in Figure 3a). When the current is higher than 120 mA, Fe^{2+} accumulation is minimal because of the low k values (close to zero). It can be calculated that the accumulation of Fe^{2+} is insignificant when the current is higher

than 85 mA.

Figure 3b shows that the accumulation of Fe^{2+} at 50 mA with different pHs also follows pseudo-first-order kinetics, giving the quantitative relationship of $k = 5.3 \times 10^4 \bullet 10^{-2pH} - 8.8 \times 10^{11} \bullet 10^{2pH-28} - 3.6 \times 10^3$ when I = 50 mA in eq. 13. The rate constant of Fe^{2+} accumulation decreases from 0.022 to 0.00001 min^{-1} as the solution pH increases from 2 to 7 (inset in Figure 3b). Similar results were found for currents of 0, 20, and 80 mA (Figure S8). This suggests that high pH inhibits the corrosion of the iron cathode at a specific current (Figure S2).[29] When the solution pH was elevated to 5.7, Fe^{2+} did not accumulate significantly, which is consistent with the fact that minimal Fe^{2+} accumulates at pH 7 at any applied current (Figure S8). The relatively high correlation coefficients ($R^2 > 0.934$) suggest that the kinetic model (eq. 13) is reasonable for Fe^{2+} accumulation.

The accumulation of Fe^{2+} at different currents and pHs is calculated and depicted in Figure 3c. A quantitative relationship between current and pH is found to be pH = 4.12 – log (I)/2 ($I \neq 0$) when k is set at zero in eq. 13. When the pH value is above the curve, no Fe^{2+} accumulates (region 1 in Figure 3c). In contrast, when the pH value is below the curve, the value of k is negative, implying that the rate of Fe^{2+} consumption is faster than that of generation (region 2 in Figure 3c).

Electrochemically Regulated Fe^{2+} Generation in a Three-electrode Column. For this study, a modified three-electrode column[13] using an iron cathode (Figure 1) was configured to regulate the localized pH around the iron cathode for generation of Fe^{2+} by adjusting the current partition between cathodes 1 (iron cathode) and 2. When

285 the current applied on the iron cathode increased from 30 to 50 mA, the pH in the
286 vicinity of iron cathode increased slightly from 3.0 to 3.5 (Figure 4a). With the current
287 further raised to 80 mA, the localized pH remarkably increases to 8. An exponential
288 relationship (eq. 14) between the pH and current is observed for the iron cathode zone
289 (inset in Figure 4a). This monotone function indicates that the localized pH is
290 determined by the current applied on the iron cathode, which differs from the batch
291 experiments where the pH is adjusted manually.

292 $$pH = 1.3 \bullet \exp(I_{iron}) \ (30 \leq I \leq 80 \text{ mA}) \qquad R^2 = 0.973 \qquad (14)$$

293 As the localized pH is determined by the current on the iron cathode, accumulation
294 of Fe^{2+} can be exclusively regulated by the current by substituting eq. 14 into eq. 13.
295 Figure 4b shows that the steady-state Fe^{2+} concentration along the column decreases
296 from maximum values in the iron cathode zone to the low values in both sides of the
297 iron cathode. It should be noted that minimal Fe^{2+} were observed around cathode 2
298 because of the neutral or alkaline conditions.[23] Cumulative Fe^{2+} concentrations in the
299 vicinity of the iron cathode at different current partitions follow in the order of 30:50 >
300 40:40 > 50:30 > 60:20 > 80:0. This was confirmed by a slight decrement as the
301 current on the iron cathode increased from 30 to 50 mA (inset in Figure 4b), followed
302 by a dramatic decrease to a low value below the detection limit as the current
303 increased to 80 mA. Decreasing the current on the iron cathode speeds up Fe^{2+}
304 generation. However, excess Fe^{2+} may consume H_2O_2 and quench •OH,[12,13,16-18,23] and
305 a low current on the iron cathode can lead to an alkaline effluent. It is important to
306 keep the current on the iron cathode at appropriate levels for generating the required

dosage of Fe^{2+}.

MTBE Transformation in the Column. In the three-electrode column using an iron cathode, MTBE (10 mg/L) transformation attains steady state after 150 min of operation (1.4 PVs) in a typical column (Figure S9). As shown in Figure 4c, MTBE can be efficiently transformed through the Pd zone. With the five ratios of current partition, the removal rates of MTBE are in the sequence 50:30 > 30:50 > 40:40 > 60:20 > 80:0, implying the critical role of current partition on MTBE transformation. The anodic current generates O_2 and H^+ (eq. 1), and the cathodic current partitioned on the iron (first cathode) generates H_2 and OH^- (eq. 2). As the quantity of H^+ produced at the anode is more than that of OH^- produced at iron (first cathode), and the reflux of OH^- from cathode 2 is complex, a low pH in local Pd zone was automatically developed, which contributes to the production of Fe^{2+} (eq. 7), H_2O_2 (eq. 3) and •OH (eq. 4). The lowest transformation of MTBE at the current ratio of 80:0 is likely result of the minimal generation of •OH from Fe^{2+} and H_2O_2 under alkaline conditions (pH 8).[23] The low efficiency of transformation at the current ratio of 60:20 is a result of the low concentrations of Fe^{2+} and H_2O_2 at pH 5.[16] At the current ratio of 30:50, the higher Fe^{2+} concentration generated competes with MTBE for •OH.[17,18,23] Although similar efficiencies were obtained for current ratios of 50:30 and 40:40, the effluent is alkaline (Figure 4a) and the energy consumption is higher for the latter ratio (Table S1).

Long-term Performance for MTBE Transformation. The long-term MTBE transformation performance of the three-electrode column using an iron cathode is

also evaluated. Figure 5 shows that MTBE transformation can be sustained at a stable level of around 70% for 20 days. About 30–40% MTBE is transformed in the anodic zone (Ports 1 and 2), which may be caused by the fact that certain Fe^{2+} and H_2O_2 produced in the iron cathode zone diffuses into the anode zone under the localized acidic condition. This finding suggests that the reaction zone was extended by convection-dispersion effects. The localized pH in the iron cathode zone decreases from 6.5 to 3.5 in the first 8 h, remaining almost constant until 10 days, after which it decreased gradually to 3.3 (Figure S10). The decline of pH in the iron cathode zone is beneficial to the accumulation of Fe^{2+} and H_2O_2,[12] which enhances MTBE transformation. It is noted that the effluent pH dramatically decreases at 8 h from 8.5 to 6.5 (Figure S10). Since the transformation of MTBE does not show any significant decrease after 20 days of operation, a relatively long longevity can be proposed for the transformation of MTBE in the three-electrode column using an iron cathode.

Implications for Groundwater Remediation. In this study, an iron cathode is employed in an in situ supply of Fe^{2+} for Pd-catalytic transformation of MTBE in simulated groundwater. Kinetic analysis and experimental results show that the accumulation of Fe^{2+} can be quantitatively related to the cathodic current applied on the iron and the solution pH. In a modified three-electrode column using an iron cathode, both the pH and Fe^{2+} accumulation in the Pd vicinity are determined by the current applied on the iron cathode, and MTBE transformation can be sustained at high levels for relatively long periods of time. Fe^{2+} concentration can be exclusively regulated by the current being applied on the iron cathode, providing a flexible

approach to supplying Fe^{2+} for Pd-catalytic transformation of organic contaminants in an iron-defective aquifer. The findings of this study may also indicate a quantitative supply of Fe^{2+} for the conventional electro-Fenton process, i.e., using one iron cathode and one O_2 reduction cathode. The effective transformation of organic contaminants including dyes,[16] TCE,[12] toluene,[13] phenol[13] and MTBE was successfully achieved by the hybrid electrolysis and Pd-catalytic oxidation process. However, a quantitative description of the transformation kinetics is still lacking. Future work will look to develop a one-dimensional reactive transport model that will describe the transformation process and guide laboratory and field remediation design.

Supporting Information Available

Additional information: Figures S1–S10, and Tables S1. This material is available free of charge via the Internet at http://pubs.acs.org.

ACKNOWLEDGEMENTS

This work was supported by the Natural Science Foundation of China (NSFC, No. 41172220), and the State Key Laboratory of Biogeology and Environmental Geology, China University of Geosciences (No. GBL11204).

Prepared by LLNL under Contract DE-AC52-07NA27344.

REFERENCES

(1) Cooper, W. J.; Cramer, C. J.; Martin, N. H.; Mezyk, S. P.; Shea, K. E. O., Sommtag, C. V. Free radical mechanisms for the treatment of methyl tert-butyl ether

(MTBE) via advanced oxidation/reductive processes in aqueous solutions. *Chem. Rev.* **2009**, *109*, 1302–1345.

(2) Hunkeler, D.; Butler, B. J.; Aravena, R.; Barker, J. F. Monitoring biodegradation of methyl tert-butyl ether (MTBE) using compound-specific carbon isotope analysis. *Environ. Sci. Technol.* **2001**, *35*, 676–681.

(3) Acero, J. L.; Handerlein, S. B.; Schmidt, T. C.; Suter, M. J. F.; Gunten, U. V. MTBE oxidation by conventional ozonation and the combination ozone/hydrogen peroxide: Efficiency of the processes and bromate formation. *Environ. Sci. Technol.* **2001**, *35*, 4252–4259.

(4) Cooper, W. J.; Tobien, T.; Nickelsen, M. G.; Adams, J. W.; Shea, K. E. O.; Bartels, D. M.; Wishart, J. F.; Tornatore, P. M.; Newman, K. S.; Gregoire, K. Radiation chemistry of methyl tert-butyl ether in aqueous solution. *Environ. Sci. Technol.* **2004**, *38*, 3994–4001.

(5) Yazaydin, A. O.; Thompson, R. W. Molecular simulation of the adsorption of MTBE in silicalite, mordenite, and zeolite beta. *J. Phys. Chem. B* **2006**, *110*, 14458–14462.

(6) Tsitonaki, A.; Petri, B.; Crimi, M.; Mosbaek, H.; Siegrist, R. L.; Bjerg, P. L. In situ chemical oxidation of contaminated soil and groundwater using persulfate: A review. *Crit. Rev. Environ. Sci. Technol.* **2010**, *40*, 55−91.

(7) Johnson, D, C.; Shamamian, V. A.; Callahan, J. H.; Denes, F. S.; Manolache, S. O.; Dandy, D. S. Treatment of methyl tert-butyl ether contaminated water using a dense medium plasma reactor: A mechanistic and kinetic investigation. *Environ. Sci.*

Technol. **2003**, *37*, 4804–4810.

(8) Stefan, M. I.; Mack, J.; Bolton, J. R.; Corporation, C. C. Degradation pathways during the treatment of methyl tert-butyl ether by the UV/H_2O_2 process. *Environ. Sci. Technol.* **2000,** *34*, 650–658.

(9) Wu, T. N. Electrocatalytic oxidation of methyl tert-butyl ether (MTBE) in aqueous solution at a nickel electrode. *Chemosphere* **2007**, *69*, 271–278.

(10) Waul, C.; Arvin, E.; Schmidt, J. E. Modeling the competitive effect of ammonium oxidizers and heterotrophs on the degradation of MTBE in a packed bed reactor. *Water Res.* **2008**, *42*, 3098–3108.

(11) Waul, C.; Arvin, E.; Schmidt, J. E. Model description and kinetic parameter analysis of MTBE biodegradation in a packed bed reactor. *Water Res.* **2008**, *42*, 3122–3134.

(12) Yuan, S. H.; Mao, X. H.; Alshawabkeh, A. N. Efficient degradation of TCE in groundwater using Pd and electro-generated H_2 and O_2: A shift in pathway from hydrodechlorination to oxidation in the presence of ferrous ions. *Environ. Sci. Technol.* **2012**, *46*, 3398−3405.

(13) Yuan, S. H.; Chen, M. J.; Mao, X. H.; Alshawabkeh, A. N. A three-electrode column for Pd-catalytic oxidation of TCE in groundwater with automatic pH-regulation and resistance to reduced sulfur compound foiling. *Water Res.* **2013**, *47*, 269−278.

(14) Mao, X. H.; Ciblak, A.; Amiri, M.; Alshawabkeh, A. N. Redox control for electrochemical dechlorination of trichloroethylene in bicarbonate aqueous media.

Environ. Sci. Technol. **2011**, *45*, 6517–6523.

(15) Mao, X. H.; Yuan, S. H.; Fallahpour, N.; Ciblak, A.; Howard, J.; Padilla, I.; Loch-caruso, R.; Alshawabkeh, A. N. Electrochemically induced dual reactive barriers for transformation of TCE and mixture of contaminants in groundwater. *Environ. Sci. Technol.* **2012**, *46*, 12003−12011.

(16) Yuan, S. H.; Fan, Y.; Zhang, Y. C.; Tong, M.; Liao, P. Pd-catalytic in situ generation of H_2O_2 from H_2 and O_2 produced by water electrolysis for the efficient electro-Fenton degradation of rhodamine B. *Environ. Sci. Technol.* **2011**, *45*, 8514−8520.

(17) Burbano, A. A.; Dionysiou, D. D.; Suidan, M. T.; Richardson, T. L. Oxidation kinetics and effect of pH on the degradation of MTBE with Fenton reagent. *Water Res.* **2005**, *39*, 107–118.

(18) Burbano, A. A.; Dionysiou, D. D.; Suidan, M. T. Effect of oxidant-to-substrate ratios on the degradation of MTBE with Fenton reagent. *Water Res.* **2008**, *42*, 3225–3239.

(19) Wang, Q.; Lemley, A. T. Kinetic model and optimization of 2,4-D degradation by anodic fenton treatment. *Environ. Sci. Technol.* **2001**, *35*, 4509–4514.

(20) Kong, L. J.; Lemley, A. T. Kinetic modeling of 2,4-dichlorophenoxyacetic acid (2,4-D) degradation in soil slurry by anodic fenton treatment. *J. Agric. Food Chem.* **2006,** *54*, 3941–3950.

(21) Joo, S. H.; Feitz, A. J.; Sedlak, D. L.; Waite, T. D. Quantification of the oxidizing capacity of nanoparticulate zero-valent iron. *Environ. Sci. Technol.* **2005**, *39*,

1263–1268.

(22) Navalon, S.; Alvaro, M.; Garcia, H. Heterogeneous fentoncatalysts based on clays, silicas and zeolites. *Appl. Catal. B Environ.* **2010**, *99*, 1–26.

(23) Brillas, E.; Sires, I.; Oturan, A. Electro-Fenton process and related electrochemical technologies based on Fenton's reaction chemistry. *Chem. Rev.* **2009**, *109*, 6570–6631.

(24) Chaplin, B. P; Reinhard, M.; Schneider, W. F.; Schuth, C.; Shapley, J. R.; Strathmann, T. J.; Werth, C. J. Critical review of Pd-based catalytic treatment of priority contaminants in water. *Environ. Sci. Technol.* **2012**, *46*, 3655−3670.

(25) He, F.; Zhao, D. Y. Hydrodechlorination of trichloroethene using stabilized Fe-Pd nanoparticles: Reaction mechanism and effects of stabilizers, catalysts and reaction conditions. *Appl. Catal. B Environ.* **2008**, *84*, 533−540.

(26) Luo, H. P.; Jin, S.; Fallgren, P. H.; Colberg, P. J. S.; Johnson, P. A. Prevention of iron passivation and enhancement of nitrate reduction by electron supplementation. *Chem. Eng. J.* **2010**, *160*, 185−189.

(27) Henderson, A. D.; Demond, A. H. Long-term performance of zero-valent iron permeable reactive barriers: A critical review. *Environ. Eng. Sci.* **2007**, *24*, 401−423.

(28) Alonso, F.; Beletskaya, I. P.; Yus, M. Metal-mediated reductive hydrodehalogenation of organic halides. *Chem. Rev.* **2002**, *102*, 4009−4091.

(29) Kim, S.; Kim, J.; and Moon. I. Parameter-based model for the forecasting of pipe corrosion in refinery plants. *Ind. Eng. Chem. Res.* **2011**, *50*, 12626–12629.

(30) Sudrabin, L. P.; Marks, H. C. Cathodic protection of steel in contact with

461 water. *Ind. Eng. Chem.*, **1952**, *44*, 1786–1791.

462 (31) Pedeferri, P. Cathodic protection and cathodic prevention. *Constr. Build.*
463 *Mater.* **1996**, *10*, 391–402.

464 (32) Metwally, I. A.; Al-Mandhari, H. M.; Nadir, A. G. Factors affecting
465 cathodic-protection interference. *Eng. Anal. Bound. Elem.* **2007**, *31*, 485–493.

466 (33) Guillard, C.; Charton, N.; Pichat, P. Degradation mechanism of *t*-butyl methyl
467 ether (MTBE) in atmospheric droplets. *Chemosphere* **2003**, *53*, 469–477.

468 (34) Eisenberg, G. Colorimetric determination of hydrogen peroxide. *Ind. Eng.*
469 *Chem. Anal. Ed.* **1943**, *15*, 327−328.

470 (35) Tai, C.; Peng, J. F.; Liu, J. F.; Jiang, G. B.; Zou, H. Determination of
471 hydroxyl radicals in advanced oxidation processes with dimethyl sulfoxide trapping
472 and liquid chromatography. *Anal. Chim. Acta* **2004**, *527*, 73−80.

473 (36) Komadel, P.; Stucki, J. W. Quantitative assay of minerals for iron(II) and
474 iron(III) using 1,10-phenanthroline. III. A rapid photochemical method. *Clays Clay*
475 *Miner.* **1988**, *36*, 379−381.

476 (37) Arnold, S. M.; Hickey, W. J.; Harris, R. F. Degradation of atrazine by
477 Fenton's reagent: Condition optimization and product quantification. *Environ. Sci.*
478 *Technol.* **1995**, *29*, 2083−2089.

479 (38) Buxton, G. V.; Greenstock, C. L.; Helman, W. P.; Ross, A. B. Critical review
480 of rate constants for reactions of hydrated electrons, hydrogen atoms and hydroxyl
481 radicals (•OH/•O^-) in aqueous solution. *J. Phys. Chem. Ref. Data* **1988**, *17*, 513–886.

482 (39) US EPA. *Technologies for treating MTBE and other fuel oxygenates, 2005*,

http://www.epa.gov/tio/download/remed/542r04009/542r04009.pdf.

(40) Hong, S.; Zhang, H.; Duttweiler, C. M.; Lemley, A. T. Degradation of methyl tertiary-butyl ether (MTBE) by anodic Fenton treatment. *J. Hazard. Mater.* **2007**, *144*, 29–40.

(41) Liang, C.; Guo, Y. Y.; Chien, Y. C.; Wu, Y. J. Oxidative degradation of MTBE by pyrite-activated persulfate: Proposed reaction pathways. *Ind. Eng. Chem. Res.* **2010**, *49*, 8858–8864.

(42) Uhlig, H. H.; Revie, R. W. *Corrosion and Corrosion Control*, John Wiley: New York, 1985.

(43) Bergendahl, J. A.; Thies, T. P. Fenton's oxidation of MTBE with zero-valent iron. *Water Res.* **2004**, *38*, 327–334.

(44) Fontes, D. E.; Mills, A. L.; Hornberger, G. M.; Herman, J. S. Physical and chemical factors influencing transport of microorganisms through porous-media. *Appl. Environ. Microbiol.* **1991**, *57*, 2473–2481.

Figure captions

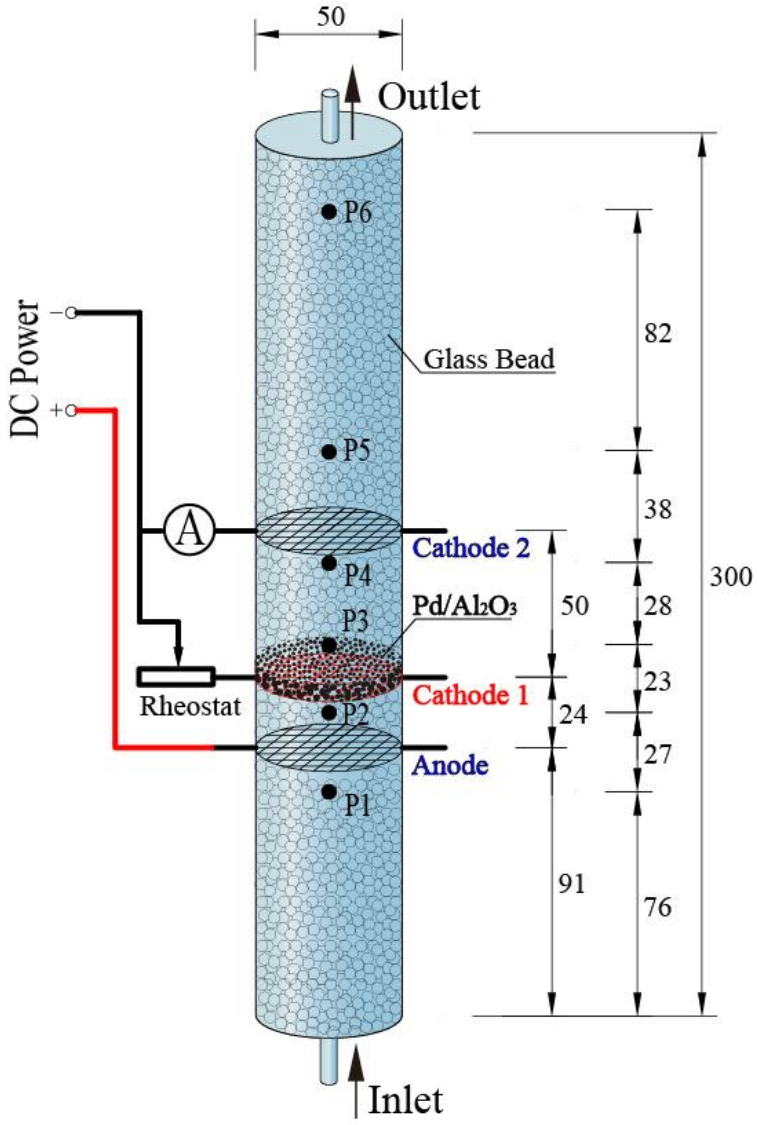

Figure 1 A schematic of the modified three-electrode column using an iron cathode. P1 to P6 refers to six sample ports. The unit of dimensions is in millimeters.

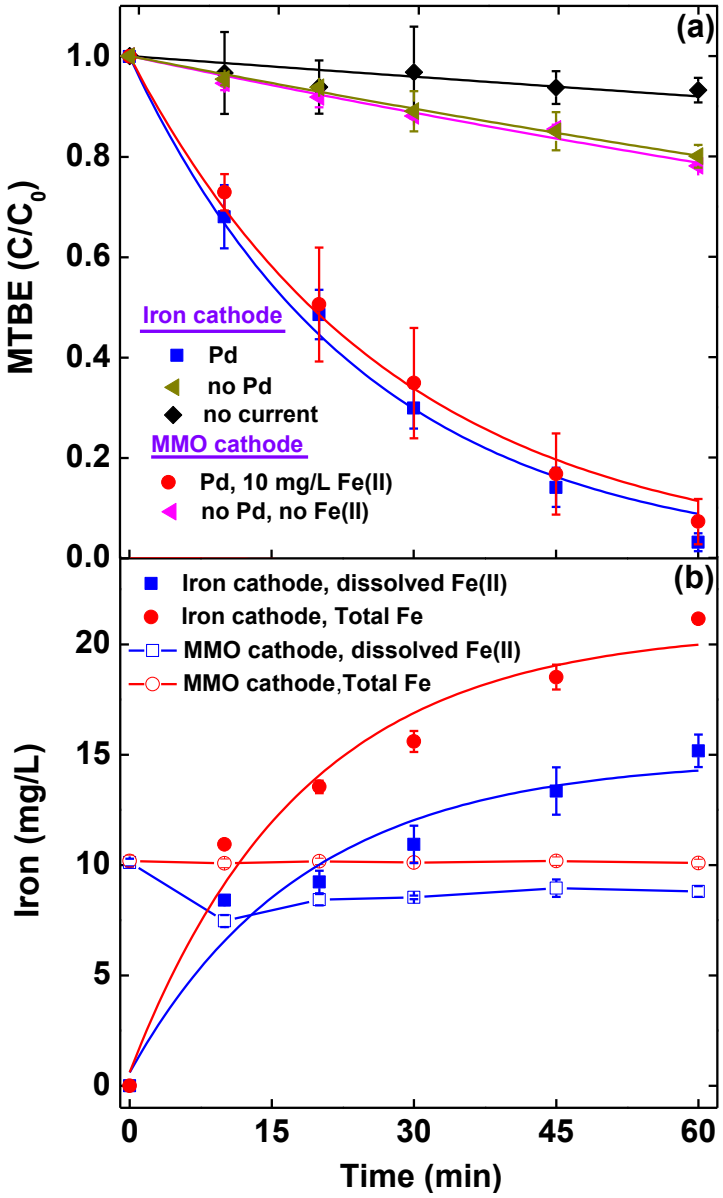

503

504 **Figure 2** (a) Transformation of MTBE and (b) variations of iron species concentration
505 in the electrolytic cell. The reaction conditions using the iron cathode are based on 20
506 mg/L initial MTBE concentration, pH 3.0, 1 g/L Pd/Al_2O_3 and 10 mM Na_2SO_4
507 background electrolyte. The reaction conditions using the MMO cathode are the same
508 as using the iron cathode except that 10 mg/L Fe^{2+} was added. Curves refer to
509 pseudo-first-order kinetic fittings. Error bars indicate 95% confidence intervals.

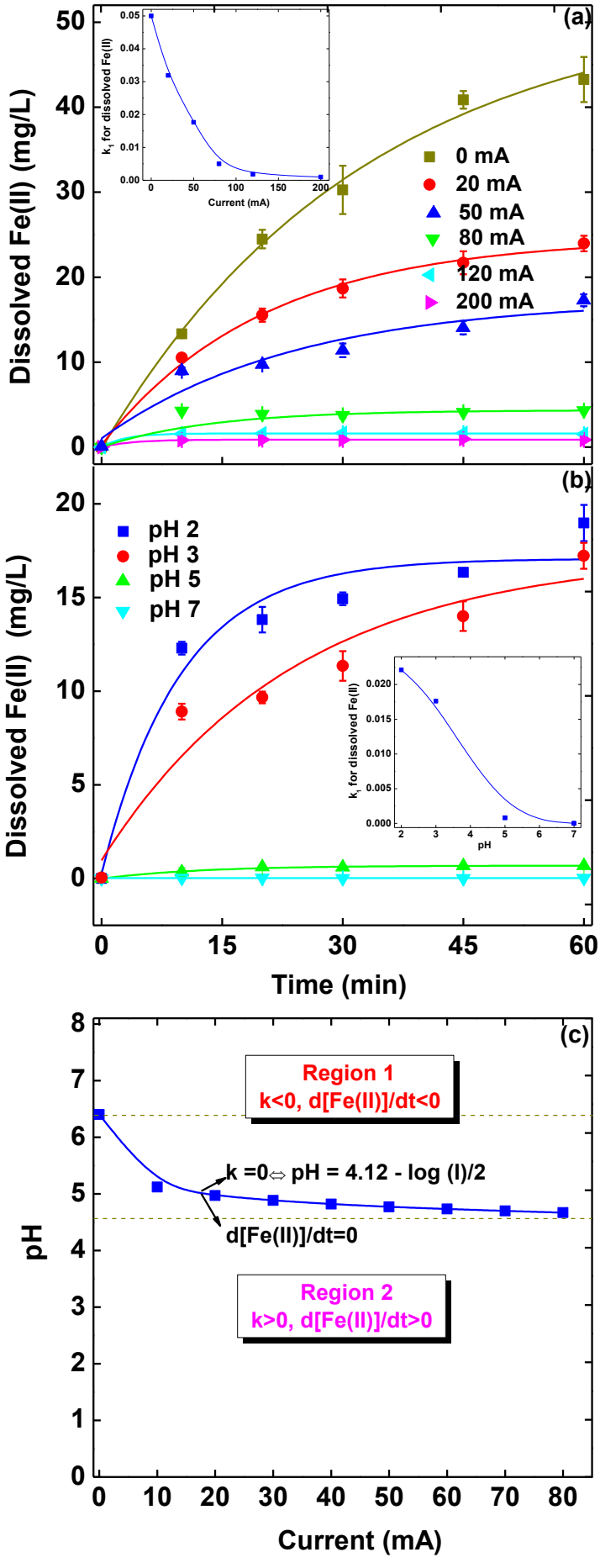
(a)
Dissolved Fe(II) (mg/L)
0 mA
20 mA
50 mA
80 mA
120 mA
200 mA
k1 for dissolved Fe(II)
Current (mA)
(b)
Dissolved Fe(II) (mg/L)
pH 2
pH 3
pH 5
pH 7
k1 for dissolved Fe(II)
pH
Time (min)
(c)
Region 1
k<0, d[Fe(II)]/dt<0
k =0⇔ pH = 4.12 - log (I)/2
d[Fe(II)]/dt=0
Region 2
k>0, d[Fe(II)]/dt>0
pH
Current (mA)

510

Figure 3 Effects of (a) current and (b) pH on accumulation of Fe^{2+} using the iron cathode, and (c) relationship of current and pH for accumulation of Fe^{2+}. Unless otherwise specified, the reaction conditions are based on pH 3, 50 mA current and 10 mM Na_2SO_4 background electrolyte. Curves refer to pseudo-first-order kinetic fittings. The insets in (a) and (b) illustrate the pseudo-first-order rate constants of Fe^{2+} accumulation versus current and pH, respectively. Error bars indicate 95% confidence intervals.

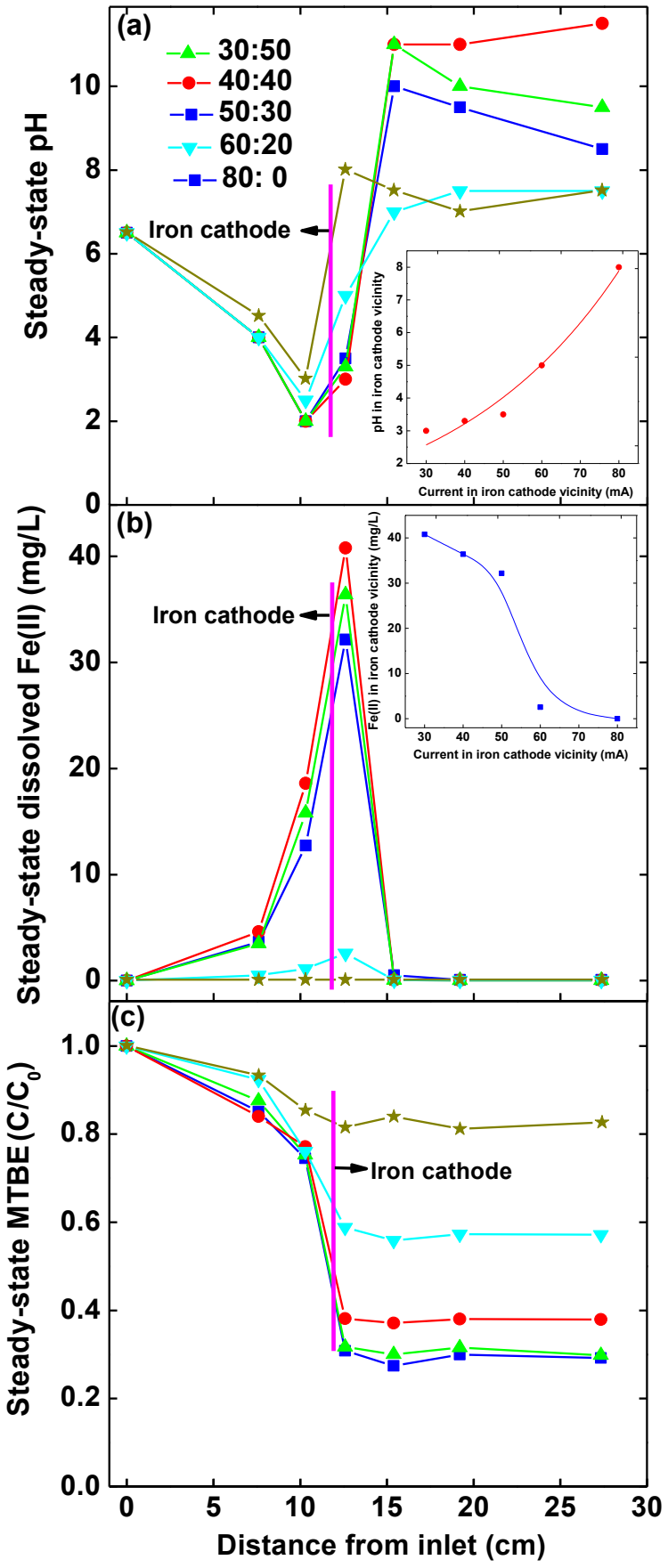

518

519 **Figure 4** Effects of current partition on the steady-state variations of (a) MTBE, (b)

pH and (c) dissolved Fe^{2+} concentration along the column. The inset in (b) illustrates the linear regression between pH and current in the vicinity of iron cathode. The inset in (c) denotes the linear regression between Fe^{2+} concentration and current in the vicinity of iron cathode. Operation conditions are based on 10 mg/L initial MTBE concentration, 2.5 mL/min and a total current of 80 mA with different partitions in cathodes 1 and 2.

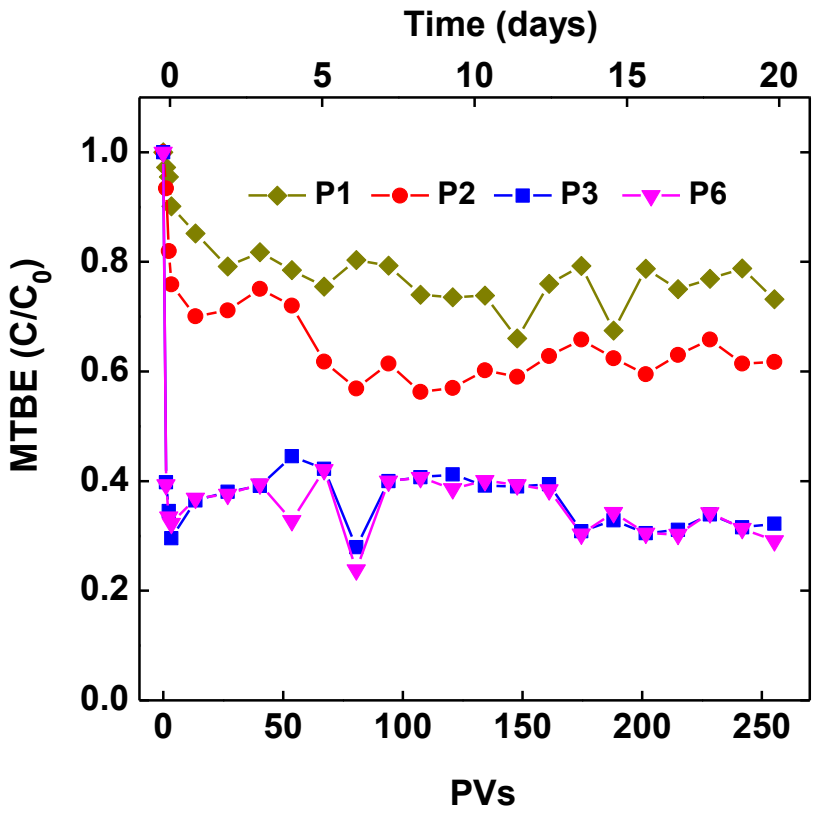

Figure 5 Long-term performance of the three-electrode column using an iron cathode for MTBE transformation. P1, P2, P3 and P6 denote different sampling ports (see Figure 1 for details). Operation conditions are based on 10 mg/L initial MTBE concentration, 2.5 mL/min and a total current of 80 mA with 50 and 30 mA partitioned in cathodes 1 and 2, respectively.

Supporting Information

Regulation of Electrochemically Generated Ferrous Ions from an Iron Cathode for Pd-Catalytic Transformation of MTBE in Groundwater

Peng Liao[†], *Songhu Yuan*[*,†], *Mingjie Chen*[‡], *Man Tong*[†], *Wenjing Xie*[†], *Peng Zhang*[†]

[†]State Key Lab of Biogeology and Environmental Geology, China University of Geosciences, 388 Lumo Road, Wuhan 430074, P. R. China

[‡]Atmospheric, Earth and Energy Division, Lawrence Livermore National Laboratory, P.O. Box 808, L-184, Livermore, CA 94550, United States

Supporting information includes 10 figures and 1 table.

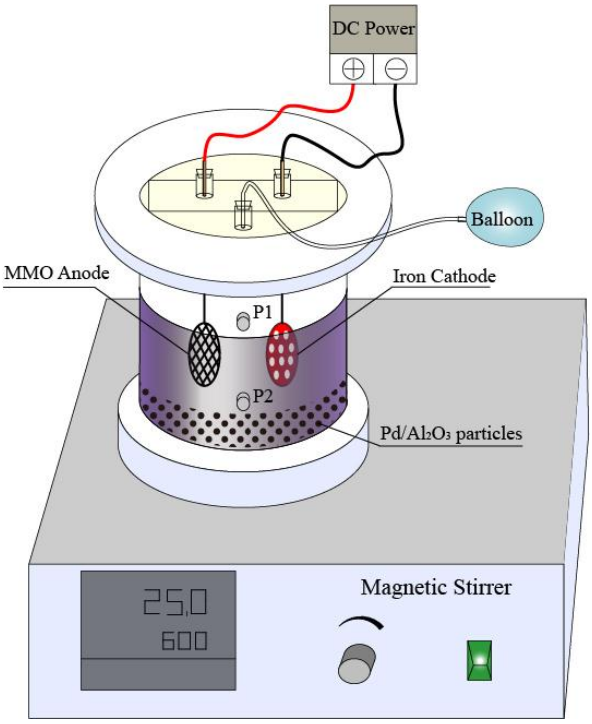

Figure S1 Experimental setup used for MTBE degradation.

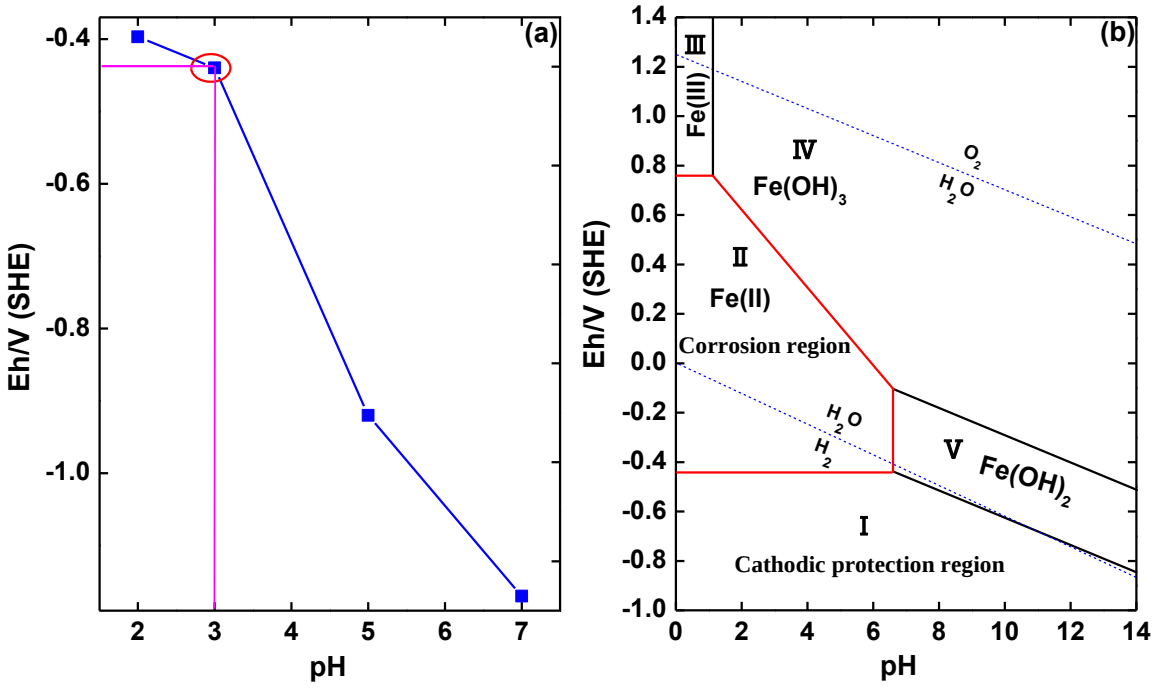

Figure S2 (a) The corrosion potentials of the iron electrode at different pHs, and (b) Eh-pH diagram for the Fe-H_2O system at 298 K.[1]

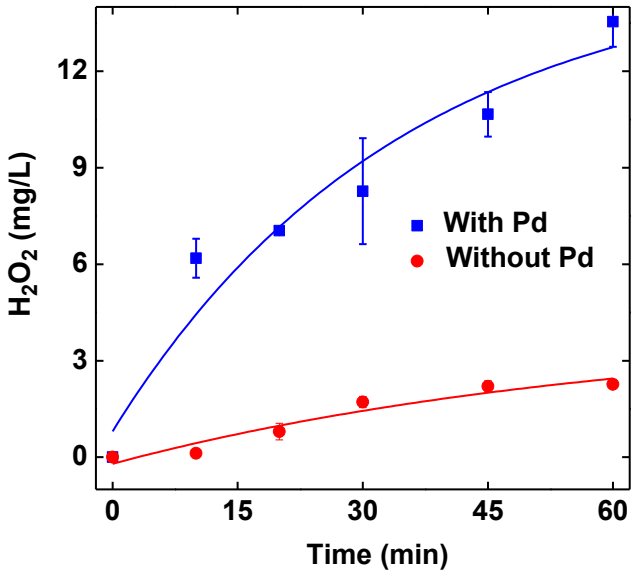

554

555 **Figure S3** H_2O_2 production using the MMO cathode in the batch experiment. The
556 reaction conditions are based on 20 mg/L initial MTBE concentration, pH 3.0, 1 g/L
557 Pd/Al_2O_3 and 10 mM Na_2SO_4 background electrolyte. Curves refer to
558 pseudo-first-order kinetic fittings. Error bars indicate 95% confidence intervals.

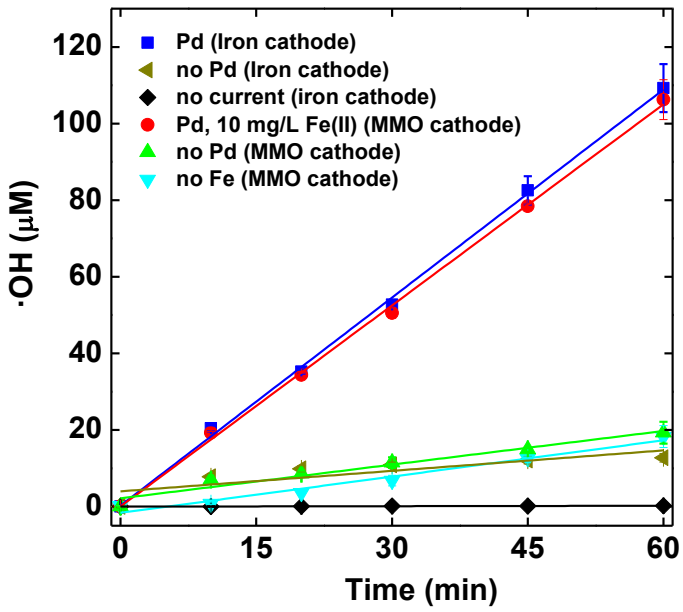

559

560 **Figure S4** Cumulative •OH concentrations under different conditions. The reaction

conditions are the same as in Figure 2 in the manuscript. Lines refer to pseudo-zero-order kinetic fittings, which is given by $C_t = k_0 t$, where *t* is the reaction time (min), k_0 is the zero-order rate constant (μM/min), and C_0 and C_t are the concentrations (μM) at times of t = 0 and t = t, respectively. Error bars indicate 95% confidence intervals.

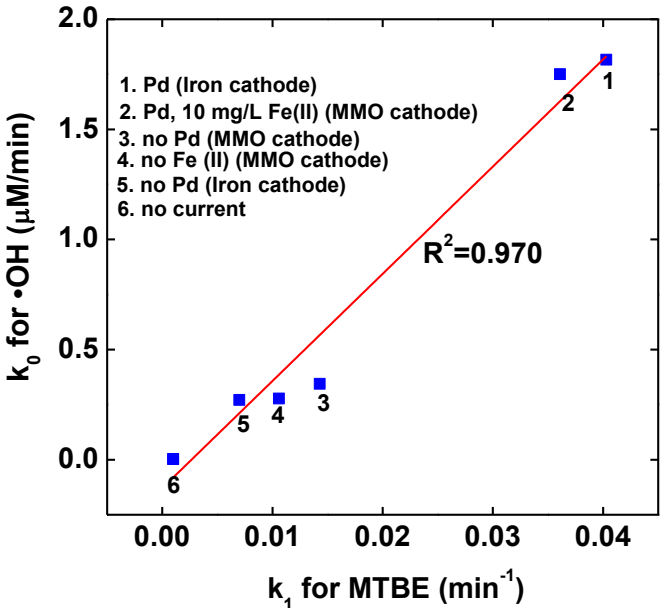

Figure S5 Correlation of •OH production rate constants with MTBE transformation rate constants.

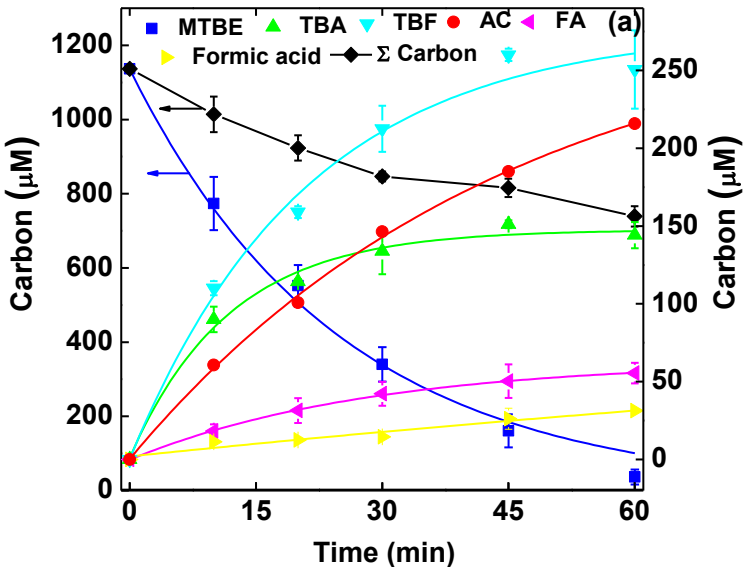

570

571 **Figure S6** Transformation profiles of MTBE using the iron cathode. The reaction

572 conditions are the same as in Figure 2 in the manuscript.

573

574

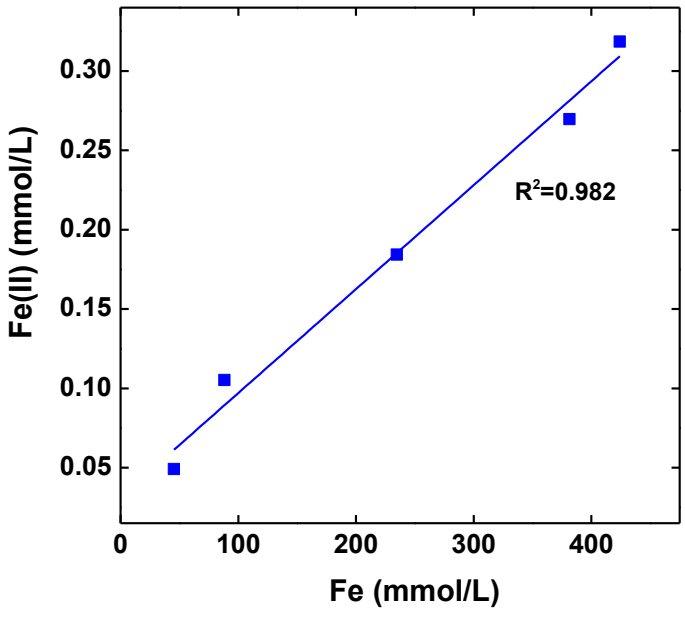

575

576 **Figure S7** Correlation of Fe(II) concentration with Fe concentration. The reaction

577 conditions are based on pH 3, 50 mA current, 10 mM Na_2SO_4 background electrolyte,

578 and 60 min reaction. The different Fe concentrations are expressed by the different
579 surface areas of the iron electrode immersed in the solution.
580

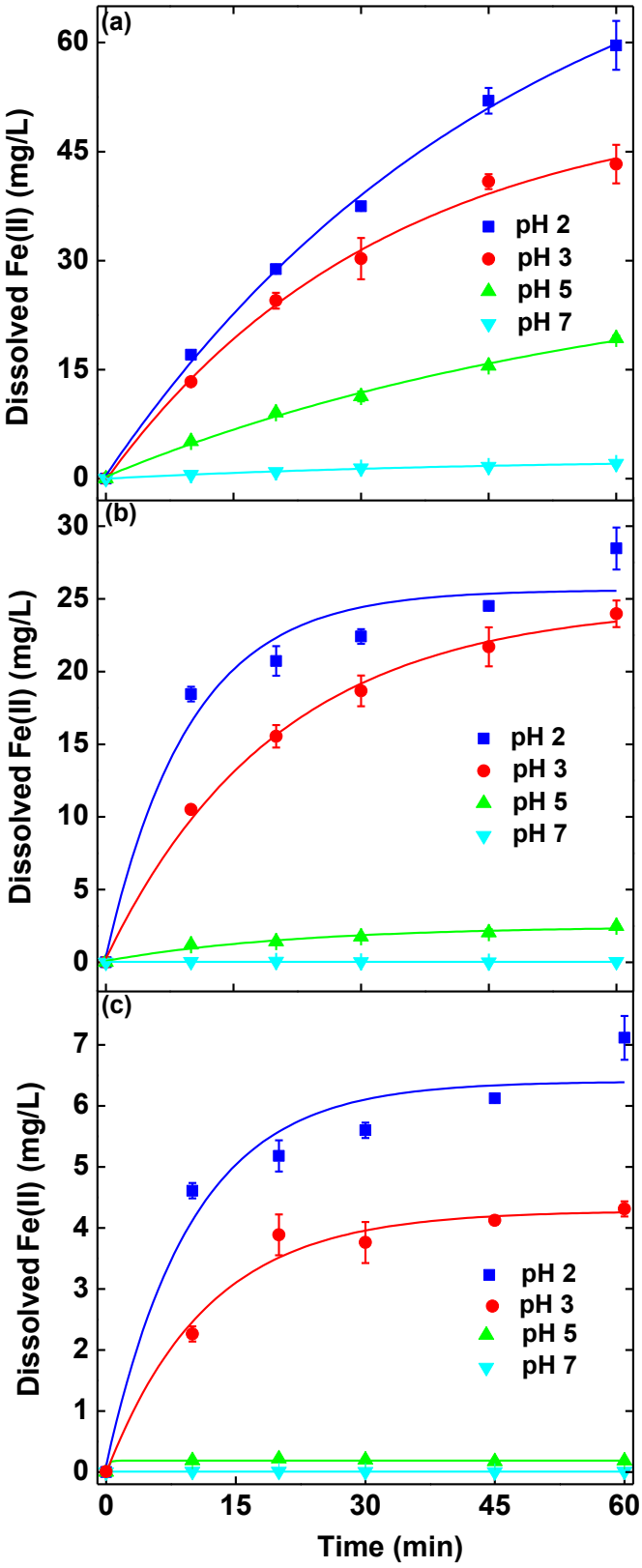

581

582 **Figure S8** Effect of pH on the accumulation of Fe(II) using the iron cathode at (a) 0,

583 (b) 20 and (c) 80 mA. The reaction conditions are based on 10 mM Na_2SO_4

584 background electrolyte. Curves refer to pseudo-first-order kintic fittings. Error bars
585 indicate 95% confidence intervals.

586

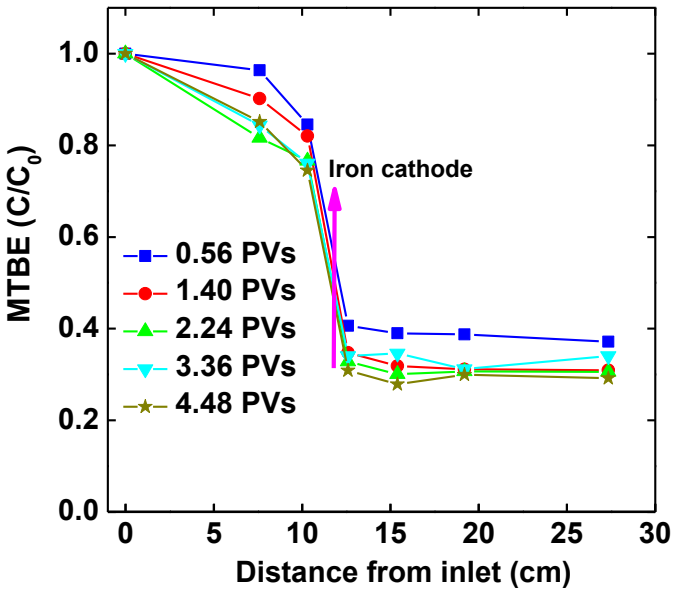

587

588 **Figure S9** Typical variations of MTBE concentrations versus time in the column.
589 Operation conditions are based on 10 mg/L initial MTBE concentration, 2.5 mL/min
590 and a total current of 80 mA with 50 and 30 mA partitioned in cathodes 1 and 2,
591 respectively.

592

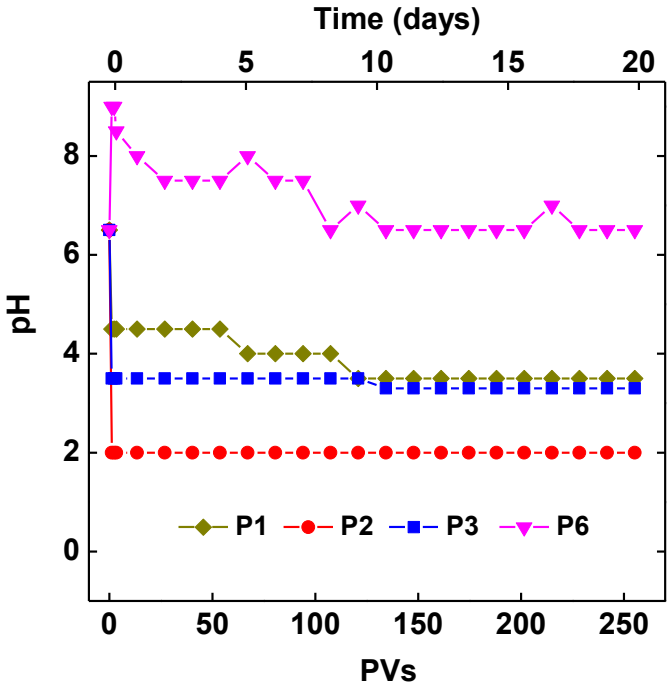

593

594 **Figure S10** Variations of pH in the modified three-electrode column using an iron

595 cathode. P1, P2, P3 and P6 denote different sample ports (See Figure 1 for details).

596 Operation conditions are the same as in Figure 5 in the manuscript.

Table S1 Parameters and Results Associated with the Column Experiments.

No.[a]	Column description	Steady-state pH		Transformation efficiency[b] (%)	Cell voltage (V)	Energy consumption ($kW•h/g_{(MTBE)}$)
		Iron cathode vicinity	Effluent			
C1	Pd/Al_2O_3, no current	6.5–7	6.5–7	4	—	—
C2	no Pd/Al_2O_3	3.5–4.5	8.5–9	35	23.8–29.3	1.8–2.2
C3	Pd/Al_2O_3	3.5–4	8–8.5	70.9	22.7–28.8	0.9–1.1
C4[c]	Pd/Al_2O_3	3–3.5	11–11.5	62.1	31.7–33.4	1.2–1.3
C5[c]	Pd/Al_2O_3	3.5–4	9.5–10	70.2	30.5–31.6	1.3–1.4
C6[c]	Pd/Al_2O_3	5–5.5	7–7.5	42.8	29.4-31.5	1.8–2.0
C7[c]	Pd/Al_2O_3	7–8	7.5–8	19	17.2–18.7	1.7-1.8
C8[d]	Pd/Al_2O_3	3.5–3.2	6.5–7	70	25.6–30.2	1.0–1.2

[a]For C1–C8, 5 mM Na_2SO_4 and 0.5 mM $CaSO_4$ were dissolved in groundwater as background electrolytes. [b]Transformation efficiency refers to total removal percentages of MTBE in the columns under steady state. [c]The cathode current partitions between cathodes 1 and 2 from C4 to C7 are

30:50, 40:40, 60:20, and 80:0, respectively. [d]A much longer period of 20 d is lasted. Unless otherwise specified, the operation conditions are based on 10 mg/L initial MTBE concentration and 2.5 mL/min, and the total current of 80 mA is applied in cathodes 1 (50 mA) and 2 (30 mA).

References

(1) Uhlig, H. H.; Revie, R. W. *Corrosion and Corrosion Control*, John Wiley: New York, 1985.